Article

Carbon–Carbon Bond Activation of 2,2,6,6-Tetramethyl-piperidine-1-oxyl by a Rh Metalloradical: A Combined Experimental and Theoretical Study

Kin Shing Chan, Xin Zhu Li, Wojciech I. Dzik, and Bas de Bruin

J. Am. Chem. Soc., **2008**, 130 (6), 2051-2061 • DOI: 10.1021/ja078157f

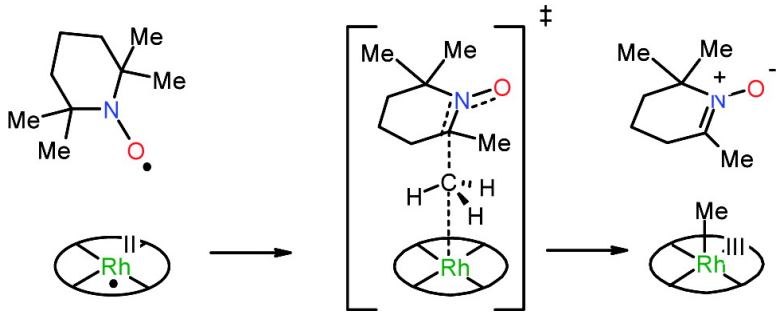

More About This Article

Additional resources and features associated with this article are available within the HTML version:

- Supporting Information
- Links to the 1 articles that cite this article, as of the time of this article download
- Access to high resolution figures
- Links to articles and content related to this article
- Copyright permission to reproduce figures and/or text from this article

View the Full Text HTML

J|A|C|S
ARTICLES
Published on Web 01/19/2008

Carbon−Carbon Bond Activation of 2,2,6,6-Tetramethyl-piperidine-1-oxyl by a Rh^{II} Metalloradical: A Combined Experimental and Theoretical Study

Kin Shing Chan,*,† Xin Zhu Li,† Wojciech I. Dzik,‡ and Bas de Bruin*,‡

Department of Chemistry, The Chinese University of Hong Kong, Shatin, New Territories, Hong Kong, People's Republic of China, and Department of Homogeneous and Supramolecular Catalysis, Van't Hoff Institute for Molecular Sciences (HIMS), University of Amsterdam, Nieuwe Achtergracht 166, 1018 WV, Amsterdam

Received October 24, 2007; E-mail: ksc@cuhk.edu.hk; bdebruin@science.uva.nl

Abstract: Competitive major carbon−carbon bond activation (CCA) and minor carbon−hydrogen bond activation (CHA) channels are identified in the reaction between rhodium(II) meso-tetramesitylporphyrin [Rh^{II}(tmp)] (**1**) and 2,2,6,6-tetramethyl-piperidine-1-oxyl (TEMPO) (**2**). The CCA and CHA pathways lead to formation of [Rh^{III}(tmp)Me] (**3**) and [Rh^{III}(tmp)H] (**5**), respectively. In the presence of excess TEMPO, [Rh^{II}(tmp)] is regenerated from [Rh^{III}(tmp)H] with formation of 2,2,6,6-tetramethyl-piperidine-1-ol (TEMPOH) (**4**) via a subsequent hydrogen atom abstraction pathway. The yield of the CCA product [Rh^{III}(tmp)Me] increased with higher temperature at the cost of the CHA product TEMPOH in the temperature range 50−80 °C. Both the CCA and CHA pathways follow second-order kinetics. The mechanism of the TEMPO carbon−carbon bond activation was studied by means of kinetic investigations and DFT calculations. Broken symmetry, unrestricted b3-lyp calculations along the open-shell singlet surface reveal a low-energy transition state (**TS1**) for direct TEMPO methyl radical abstraction by the Rh^{II} radical (S_H2 type mechanism). An alternative ionic pathway, with a somewhat higher barrier, was identified along the closed-shell singlet surface. This ionic pathway proceeds in two sequential steps: Electron transfer from TEMPO to [Rh^{II}(por)] producing the [TEMPO]$^+$[Rh^{I}(por)]$^-$ cation−anion pair, followed by net CH_3^+ transfer from TEMPO$^+$ to Rh^I with formation of [Rh^{III}(por)Me] and (DMPO-like) 2,2,6-trimethyl-2,3,4,5-tetrahydro-1-pyridiniumolate. The transition state for this process (**TS2**) is best described as an S_N2-like nucleophilic substitution involving attack of the d_z2 orbital of [Rh^{I}(por)]$^-$ at one of the $C_{Me}-C_{ring}$ σ^* orbitals of [TEMPO]$^+$. Although the calculated barrier of the open-shell radical pathway is somewhat lower than the barrier for the ionic pathway, R-DFT and U-DFT are not likely comparatively accurate enough to reliably distinguish between these possible pathways. Both the radical (S_H2) and the ionic (S_N2) pathway have barriers which are low enough to explain the experimental kinetic data.

Introduction

Carbon-carbon bond activation (CCA) by a transition metal complex is much less frequently observed than C−H bond activation (CHA).[1] It has been commonly accepted that C−C bond activation is sterically more demanding than C−H bond activation.[1] Furthermore, C−H bonds are statistically more abundant than C−C bonds in most substrates, thereby favoring CHA. Among the C−C bonds, aliphatic CCA is sterically most demanding and difficult. Examples are rarely encountered in unstrained systems.[1]

Although CCA is kinetically less favorable than CHA, it is thermodynamically possible and competitive especially for late transition metal complexes in which M−C bonds are stronger or comparable in strength compared to M−H bonds.[2] Examples of unstrained, non-aliphatic CCA and CHA have been reported in the reactions of $Mn_2(CO)_{10}$ with pentamethylcyclopentadiene,[3] in Rh−PCP and Ir−PCP systems,[4] and for a Ni−allyl cyanide complex.[5]

The rich chemistry of Rh^{II} and Ir^{II} has been extensively studied.[6,7] In our groups we have a strong focus on gaining a

† Chinese University of Hong Kong.
‡ University of Amsterdam.

(1) (a) Crabtree, R. H. *Chem. Rev.* **1985**, *85*, 245−269. (b) Murakami, M.; Ito, Y. In *Topics in Organometallic Chemistry*; Murai, S., Ed.; Springer: Berlin 1999; Vol. 3, pp 97−129. (c) Rybtchinski, B.; Milstein, D. *Angew. Chem. Int. Ed.* **1999**, *38*, 870−883. (d) Jun, C.-H. *Chem. Soc. Rev*. **2004**, *33*, 610−618.
(2) Martinho Simões, J. A.; Beauchamp, J. L. *Chem. Rev.* **1990**, *90*, 629−688.
(3) Hemond, R. C.; Hughes, R. P.; Locker, H. B. *Organometallics* **1986**, *5*, 2391−2392.
(4) (a) Rybtchinski, B.; Vigalok, A.; Ben-David, Y.; Milstein, D. *J. Am. Chem. Soc.* **1996**, *118*, 12406−12415. (b) Sundermann, A.; Uzan, O.; Milstein, D.; Martin, J. M. L. *J. Am. Chem. Soc.* **2000**, *122*, 7095−7104.
(5) Brunkan, N. M.; Brestensky, D. M.; Jones, W. D. *J. Am. Chem. Soc.* **2004**, *126*, 3627−3641.
(6) (a) Cui, W. H.; Wayland, B. B. *J. Am. Chem. Soc.* **2006**, *128*, 10350−10351. (b) Cui, W. H.; Wayland, B. B. *J. Am. Chem. Soc.* **2004**, *126*, 8266−8274. (c) Cui, W.; Zhang, X. P.; Wayland, B. B. *J. Am. Chem. Soc.* **2003**, *125*, 4994−4995. (d) Zhang, X.-X.; Wayland, B. B. *J. Am. Chem. Soc.* **1994**, *116*, 7897−7898. (e) Wayland, B. B.; Ba, S.; Sherry, A. E. *J. Am. Chem. Soc.* **1991**, *113*, 5305−5311. (f) Sherry, A. E.; Wayland, B. B. *J. Am. Chem. Soc.* **1990**, *112*, 1259−1261. (g) Farnos, M. D.; Woods, B. A.; Wayland, B. B. *J. Am. Chem. Soc.* **1986**, *108*, 3659−3663.

deeper understanding of the metalloradical reactivity of several Rh^{II} and Ir^{II} radicals.[8−10] A particular unique chemistry concerns the activation of aliphatic carbon−carbon bonds in a variety of organic substrates including nitroxyl radicals,[10a,b] ketones,[10c] amides,[10d] esters,[10d] and nitriles[10e,f] by rhodium(II) meso-tetramesitylporphyrin, [Rh^{II}(tmp)] (**1**).[6e]

TEMPO (2,2,6,6-tetramethyl-piperidine-1-oxyl) is often used as a radical inhibitor in various (catalytic) reactions and can mediate transition metal-catalyzed oxidation reactions. In these reactions (the oxygen atom of) its nitroxyl radical moiety is generally believed to be responsible for its actions, and (radical mediated) decomposition reactions of TEMPO involving its aliphatic moieties are generally not considered relevant. Considering the results presented in this paper this assumption is not always justified.

In this report we focus on providing a deeper mechanistic understanding of our previously communicated CCA of unstrained CR_3-C_{ring} bonds of cyclic nitroxyl radicals by Rh^{II}.[10b] We studied in detail the kinetics of the CCA reaction of [Rh(tmp)] (**1**) with TEMPO **2** leading to [Rh^{III}(tmp)Me] (**3**). In this process we identified a competing CHA pathway leading to formation of TEMPOH via [Rh^{III}(tmp)H]. The selectivity of CCA over CHA increases at higher temperatures. Herein we disclose a detailed mechanistic picture supported by DFT calculations.

Reaction of Rh(tmp) **1** with TEMPO **2** for 4 h gives rise to formation of [Rh^{III}(tmp)Me] **3** in high yield (Scheme 1, Table 1).[10b] Careful analysis of the crude reaction mixture by GC−MS revealed the presence of 2,2,6,6-tetramethyl-piperidin-1-ol TEMPOH **4**, suggestive for a competing reaction. Other organic coproducts which can be expected to result from these reactions, such as nitrone **6** and azaoxetane **7**, proved too unstable to be detected by GC−MS or isolated (Scheme 1).[11] However, a closely related analogue of **6** was detected in the reaction of [Rh^{II}(tmp)] with 2,2- dimethyl-5,5-diphenylpyrrolidin-1-oxyl, yielding 2-methyl-2,5-diphenyl-3,4-dehydronitrone and [Rh^{III}(tmp)Me].[10b]

Scheme 1. Competing CCA and CHA TEMPO Activation Pathways upon Reaction with **1**[a]

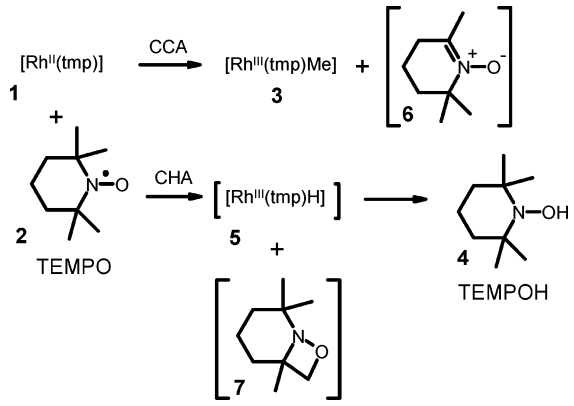

[a] Reactions in benzene under a N_2 atmosphere at 70 °C for 4 h.

Table 1. Yields of Rh(tmp)Me and TEMPOH

entry	temp °C	TEMPO equiv	% Rh(tmp)Me	% TEMPOH	% total yield	Rh(tmp)Me: TEMPOH
1	70	1	60	5.7	65.7	10.5:1
2	70	2	76	8.0	83.0	9.5:1
3	70	5	80	9.0	89.0	8.9:1
4	70	20	82	9.3	91.3	8.8:1
5	50	20	73	16.8	89.8	4.4:1
6	60	20	76	12.3	88.3	6.1:1
7	80	20	85	3.9	88.9	21.8:1

Increasing the TEMPO/Rh ratio, while keeping all other reaction conditions identical (70 °C), gives rise to increased overall yields of both Rh(tmp)Me **3** and TEMPOH **4**, but also decreases the **3**/**4** ratio. (Table 1, entries 1−4). Increasing the TEMPO/Rh ratio from 1 to 20 gradually increases the [Rh^{III}(tmp)Me] yield from 60 to 82% and the TEMPOH yield from 5.7 to 9.3%. The highest total product yields (92%) were reached using 20 equiv of TEMPO, although the yields already leveled off to 89% when using 5 equiv of TEMPO. Using more than 5 equiv TEMPO gives rise to a nearly constant **3**/**4** ratio of about 8.8.

We observed a clear influence of the temperature on the relative rates of the two competing pathways (50−80 °C). Keeping the TEMPO and [Rh^{II}(tmp)] concentrations constant while increasing the temperature results in higher yields of [Rh^{III}(tmp)Me] but lower yields of TEMPOH, thus resulting in a *higher* **3**/**4** ratio (Table 1, entries 5, 6, 4, and 7). The total product yields remained high and ascertained that other side reactions were minor.

The formation of TEMPOH and the origin of the hydroxyl hydrogen in TEMPOH atom is puzzling. It seems most likely that the reaction proceeds via the hydride intermediate [Rh^{III}(tmp)H].[12] Rh−H bonds of [Rh^{III}(por)] species are weak (∼60 kcal/mol)[6d] and can donate their hydrogen atoms easily,[12b] and TEMPO is known to react rapidly with [M^{III}(oep)H] hydride

(7) (a) Paonessa, R. S.; Thomas, N. C.; Halpern, J. *J. Am. Chem. Soc*. **1985**, *107*, 43333−4335. (b) Chen, M. J.; Rathke, J. W. *Organometallics* **1994**, *13*, 4875−4880.

(8) For recent overviews, see: (a) Hetterscheid, D. G. H.; Grützmacher, H.; Koekoek, A. J. J.; de Bruin, B. In *The Organometallic Chemistry of Rh, Ir, Pd and Pt Based Radicals; Higher Valent Species*; Karlin, K. D., Ed.; Vol 55; Wiley: 2007, pp 247−354. (b) de Bruin, B.; Hetterscheid, D. G. H. *Eur. J. Inorg. Chem*. **2007**, *2*, 211−230.

(9) (a) Hetterscheid, D. G. H.; Klop, M.; Kicken, R. J. N. A. M.; Smits, J. M. M.; Reijerse, E. J.; de Bruin, B. *Chem. Eur. J*. **2007**, *13*, 3386−3405. (b) de Bruin, B.; Russcher, J. C.; Grüzmacher, H. *J. Organomet. Chem*. **2007**, *692*, 3167−3173. (c) Hetterscheid, D. G. H.; de Bruin, B. *J. Mol. Catal. A. Chem.*, **2006**, *251*, 291−296. (d) Hetterscheid, D. G. H.; Kaiser, J.; Reijerse, E. J.; Peters, T. P. J.; Thewissen, S.; Blok, A. N. J.; Smits, J. M. M.; de Gelder, R.; de Bruin, B. *J. Am. Chem. Soc*. **2005**, *127*, 1895−1905. (e) Hetterscheid, D. G. H.; Bens, M.; de Bruin, B.; *Dalton Trans*. **2005**, 979−984. (f) Knijnenburg, Q.; Horton, A. D.; van der Heijden, H.; Kooistra, T. M.; Hetterscheid, D. G. H.; Smits, J. M. M.; de Bruin, B.; Budzelaar, P. H. M.; Gal, A. W. *J. Mol. Catal. A. Chem*. **2005**, *232*, 151−159. (g) Hetterscheid, D. G. H.; Smits, J. M. M.; de Bruin, B. *Organometallics*. **2004**, *23*, 4236−4246. (h) de Bruin, B.; Budzelaar, P. H. M.; Gal, A. W.; *Angew. Chem., Int. Ed*. **2004**, *43*, 4142−4157. (i) Hetterscheid, D. G. H.; de Bruin, B.; Smits, J. M. M.; Gal, A. W. *Organometallics* **2003**, *22*, 3022−3024. (j) de Bruin, B.; Thewissen, S.; Yuen, T.-W.; Peters, T. P. J.; Smits, J. M. M.; Gal, A. W.; *Organometallics* **2002**, *21*, 4312−4314. (k) de Bruin, B.; Peters, T. P. J.; Thewissen, S.; Blok, A. N. J.; Wilting, J. B. M.; de Gelder, R.; Smits, J. M. M.; Gal, A. W. *Angew. Chem., Int. Ed*. **2002**, *41*, 2135−2138. (l) Willems, S. T. H.; Russcher, J. C.; Budzelaar, P. H. M.; de Bruin, B.; de Gelder, R.; Smits, J. M. M.; Gal, A. W. *Chem. Commun*. **2002**, 148−149.

(10) (a) Mak, K. W.; Yeung, S. K.; Chan, K. S. *Organometallics* **2002**, *21*, 2362−2364. (b) Tse, M. K.; Chan, K. S. *J. Chem. Soc. Dalton Trans*. **2001**, 510−511. (c) Zhang, L.; Chan, K. S. *J. Organomet. Chem*. **2006**, *691*, 3782−3787. (d) Zhang, L.; Chan, K. S. *J. Organomet. Chem*. **2007**, *692*, 2021−2027. (e) Chan, K. S.; Li, X. Z.; Fung, C. W.; Zhang, L. *Organometallics* **2007**, *26*, 20−21. (f) Chan, K. S.; Li, X. Z.; Fung, C. W.; Zhang, L. *Organometallics* **2007**, *26*, 2679−2687.

(11) (a) A more stable diphenyl substituted nitrone co-product analogue of **6** has been isolated; see ref 7. (b) Breuer, E.; Aurich, H. G.; Nielsen, A. *Nitrones, Nitronates and Nitroxides:* Wiley & Sons: New York, 1989. (c) A derivative of azaoxetane **7** has been a proposed, unstable intermediate: Baldwin, J. E.; Bhatnagar, A. K.; Choi, S. C.; Shortridge, T. J. *J. Am. Chem. Soc*. **1971**, *93*, 4082−4084.

(12) (a) Chan, K. S.; Leung, Y. B. *Inorg. Chem*. **1994**, *33*, 3187. (b) Zhang, L.; Chan, K. S. *Organometalllics* **2007**, *26*, 679−684.

species (M = Rh, Ir) at room temperature to give TEMPOH and the corresponding metal dimers.[12a] Also in our hands, [Rh^{II}(tmp)H] was indeed found to react with TEMPO in benzene to give [Rh^{II}(tmp)] and TEMPOH (eq 4) in >96% yield, so formation of TEMPOH via an intermediate [Rh^{III}(tmp)H] species is a very likely pathway. However, this still leaves the question to what is source of the hydrogen atom. We considered four possible hydrogen sources: (1) the substrate TEMPO, (2) the solvent benzene, (3) the starting material [Rh^{II}(tmp)], and (4) the product [Rh^{III}(tmp)Me]. Each of these sources can have its unique hydrogen transfer mechanistic pathway. We performed some additional experiments aiming at revealing the most likely hydrogen source.

Since TEMPO proved stable in benzene at 70 °C for 24 h without any decomposition (determined by GC−MS analysis using an internal standard), we rule out a direct intermolecular hydrogen atom transfer from benzene (or another TEMPO moiety) to TEMPO.[13] Also [Rh^{II}(tmp)] is stable in benzene at 130 °C for at least 2 days.[6e,12b] Even though [Rh^{III}(tmp)Me] reacts with [Rh^{II}(tmp)] at 130 °C to give [Rh^{III}(tmp)Et] via the proposed intermediate [Rh^{III}(tmp)H],[10f] no reaction is observed at all at 70 °C. Therefore, [Rh^{III}(tmp)Me] cannot be the hydrogen source for formation of TEMPOH. Hydrogen atom transfer from benzene, [Rh^{III}(tmp)Me] or another [Rh^{II}(tmp)] moiety to [Rh^{II}(tmp)] is clearly difficult, so we can safely exclude these reagents serving as a hydrogen source for TEMPOH (sources 3 and 4). This leaves a hydrogen atom transfer pathway involving CHA of TEMPO by [Rh^{II}(tmp)] to give the [Rh^{III}(tmp)H] intermediate, which in turn transfers its hydrogen atom to another TEMPO moiety leading to TEMPOH with reformation of Rh^{II}(tmp)] (source 1 via [Rh^{III}(tmp)H]) as the most likely pathway (Scheme 1).

The formation of [Rh^{III}(tmp)H] through a chelation-assisted CHA by [Rh^{II}(tmp)] is kinetically favorable.[12b] While this C−H bond activation is apparently uphill (since a weaker Rh−H bond is formed by breaking a strong C−H bond (Rh(tmp)−H = 60 kcal/mol,[6e] Me_3CCH_2−H = 100 kcal/mol),[13] the formation of the organic coproduct azaoxetane **7** could render the process energetically favorable. Furthermore, the CHA reaction could be simply driven by the fast and favorable follow-up reaction of [Rh^{III}(tmp)H] with TEMPO to give TEMPOH and [Rh^{II}(tmp)]. This would imply that the TEMPOH yield should increase at higher TEMPO concentrations. Indeed, increasing the [TEMPO] from 1 to 20 equiv increases the TEMPOH yield. Not only in absolute sense, but the CHA pathway is also relatively more favored at higher [TEMPO] compared to the CCA, as can be derived from the decreasing **3**/**4** product ratio (Table 1, entries 1 to 4). This implies that the overall CHA activation process likely involves more equiv of TEMPO (likely 2) than the CCA process (likely 1).

Binding Studies and Kinetic Investigations. To shed some more light on the reaction mechanism, we investigated the binding affinity of TEMPO to [Rh^{II}(tmp)], the kinetics of the CCA and CHA reactions as well as the kinetics associated with the hydrogen atom transfer from [Rh^{III}(tmp)H] to TEMPO.

(13) This is understandable, because the energy of the TEMPOH O−H bond is only 70 kcal/mol and thus not strong enough to allow hydrogen atom transfer from the much stronger alkyl C−H bonds of TEMPO or benzene (Me_3CCH_2-H = 100 kcal/mol, Ph-H = 113 kcal/mol). See: Luo, Y.-R. *Handbook of Bond Dissociation Energies in Organic Compounds;* CRC Press: Boca Raton, FL, 2003.

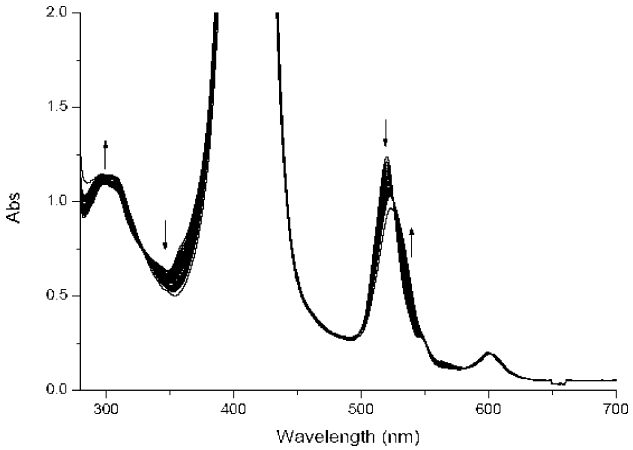

Figure 1. UV−vis titration spectra of Rh(tmp) with TEMPO at 10.0 °C.

Table 2. Summary of Spectrophotometric Titration of Rh(tmp) with TEMPO

entry	*T* (°C)	1/*T* (K^{-1})	TEMPO: Rh(tmp)	log K_1	R
1	10.0	0.00353	0.98 ± 0.02	4.62 ± 0.09	0.996
2	15.0	0.00347	1.01 ± 0.01	4.53 ± 0.06	0.999
3	20.0	0.00341	0.98 ± 0.02	4.35 ± 0.07	0.998
4	25.0	0.00336	0.98 ± 0.01	4.06 ± 0.04	0.997
5	30.0	0.00330	0.99 ± 0.01	3.93 ± 0.05	0.995
6	70.0			2.69 (extrapolated)	

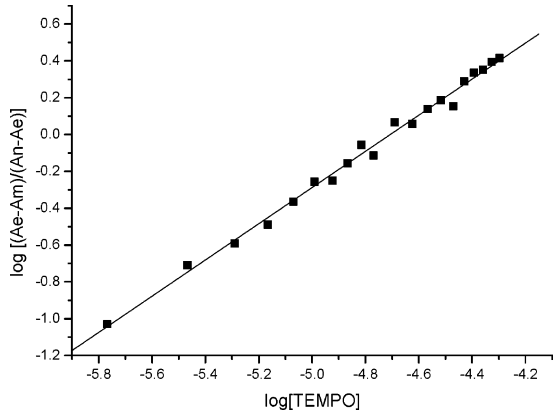

Figure 2. Measured absorbance against concentration of TEMPO added at 10 °C.

Since the yields of the CCA and CHA reactions are both dependent on the TEMPO concentration we decided to evaluate the binding constant K_1 (= k_1/k_{-1}) for TEMPO binding to [Rh^{II}(tmp)]. The binding stoichiometry and binding constant were evaluated spectrophotometrically from changes in absorbance at 521 nm in the temperature range from 10 to 30 °C (Figure 1 and Table 2). Analyses of the data confirmed a 1:1 adduct (See Figure 2, for details see Experimental Section) and yielded a binding constant K_1 (= k_1/k_{-1}) = 2.24 × 10^4 ± 1.2 M^{-1} at 20.0 °C. A van't Hoff plot of the binding constants at different temperatures provided the enthalpy and entropy values: ΔH_1 = −14.7 ± 1.4 kcal mol^{-1}, and ΔS_1 = −30.6 ± 4.6 cal mol^{-1} K^{-1} (Figure 3). The extrapolated value of K_1 at 70 °C (the reaction temperature at which the competing CCA and CHA reactions were studied) is also listed in Table 2 for a subsequent comparison with the kinetic data below.

The kinetics of the reaction between [Rh^{II}(tmp)] **1** and TEMPO **2** were investigated spectophotometrically by following

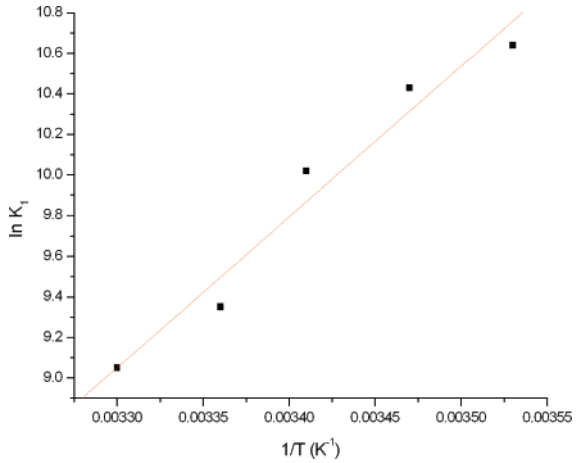

Figure 3. van't Hoff plot of binding of Rh(tmp) with TEMPO.

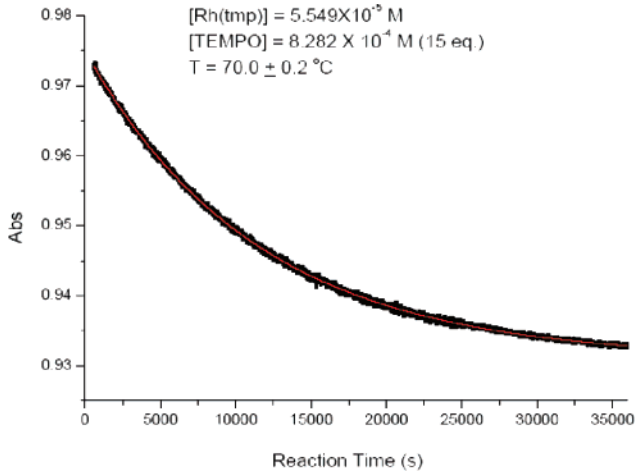

Figure 4. Typical time scan of the reaction between [Rh^{II}(tmp)] and TEMPO.

Table 3. k'_{obs} under Different TEMPO and Rh(tmp) Concentrations at 70 °C

entry	[Rh(tmp)] (10^{-5} M)	[TEMPO] (10^{-4} M)	k'_{obs} (10^{-5} s^{-1})
1	2.775	8.282	8.79 ± 0.01
2	5.549	8.282	8.74 ± 0.02
3	5.549	16.56	16.99 ± 0.05
4	5.549	24.97	24.45 ± 0.05
5	5.549	33.13	34.97 ± 0.08
6	5.549	49.70	49.47 ± 0.08

changes in the absorbance at 523 nm under the reaction conditions 70.0 °C, initial concentrations (2.775 − 8.324) × 10^{-5} M Rh(tmp) and (0.828 − 4.970) × 10^{-3} M TEMPO with TEMPO always in at least 10-fold excess. The reactions were monitored for at least four half-lives.

The kinetics conformed to first-order reactions in both [**1**] and [**2**]. The rate laws are defined in eqs 1−3. With excess TEMPO, the observed rate constants k'_{obs} (eq 3, Figure 4) were evaluated by first-order fitting of the absorbance changes and did not change with the initial concentrations of [Rh^{II}(tmp)] (Table 3, entries 1−2). The reaction order in [**1**] (*n*) is clearly equal to one. Variation of the concentration TEMPO at fixed concentration of [Rh^{II}(tmp)] yielded a linear plot (Table 3, entries 3−6, Figure 3), in good agreement with a reaction order in [**2**] (*m*) equal to one. The resulting overall rate law is shown in eq 3 where k_{obs} = 0.11 L mol^{-1} s^{-1}.

$$\text{rate} = k_{obs}[[Rh^{II}(tmp)]]^n[TEMPO]^m \quad (1)$$

$$= k'_{obs}[[Rh^{II}(tmp)]] \quad (2)$$

$$= k_{obs}[[Rh^{II}(tmp)]][TEMPO] \quad (3)$$

The temperature dependent observed rate constants k'_{obs} were measured in the temperature range from 50−80 °C and are tabulated in Table 4. An Erying plot (Figure S1) yielded the corresponding enthalpies and entropies of activation: $\Delta H_{obs}^{\ddagger}$ = 15.02 ± 0.71 kcal mol^{-1} and $\Delta S_{obs}^{\ddagger}$ = −20.93 ± 0.88 cal K^{-1} mol^{-1}. Given the product distributions in the applied temperature range (Table 1), the obtained activation parameters should mainly reflect those of the major CCA process.

To ascertain that the rate determining step of the CHA pathway is the CHA step and not the follow-up reaction, we investigated the kinetics of the reaction between [Rh^{III}(tmp)H] **5** and TEMPO **2**. TEMPO reacted with [Rh^{III}(tmp)H] at room temperature in 10 min to give TEMPOH in 96% yield as determined by GC−MS analysis (eq 4). Since [Rh^{II}(tmp)] is air-sensitive and difficult to purify, its yield was measured indirectly as [Rh^{III}(tmp)I], which is formed from [Rh^{II}(tmp)] by a subsequent reaction with added excess iodine. [Rh^{III}(tmp)I] was obtained in 93% yield (average of three runs) after column chromatography. With the assumption of quantitative yield of iodination (2 [Rh^{II}(tmp)] + I_2 → 2 [Rh^{III}(tmp)I]), the yield of [Rh^{II}(tmp)] from the reaction with TEMPO and [Rh^{III}(tmp)H] was estimated at 93% (eq 4).

$$\underset{}{Rh(tmp)H} + TEMPO \xrightarrow[\text{rt, 10 min}]{C_6H_6,\ N_2} \underset{93\%}{Rh(tmp)} + \underset{96\%}{TEMPOH} \quad (4)$$

With the follow-up hydrogen atom transfer (HAT) reaction of [Rh^{III}(tmp)H] with TEMPO being established as a clean reaction, the kinetics of the reaction were followed spectrophotometrically at 522 nm under the conditions 15.0 °C, initial concentrations (2.96−8.87) × 10^{-5} M [Rh^{III}(tmp)H] and (9.11−5.47) × 10^{-3} M TEMPO with TEMPO always in at least 10-fold excess (Table 5). The observed rate constants $k'_{HAT,obs}$ follow a first-order decay in [Rh^{III}(tmp)H] and the observed rate constants did not change with the initial concentration of [Rh^{III}(tmp)H] (Table 5, entries 1−3, Figure 5). Therefore, the kinetic order in [[Rh^{III}(tmp)H]] was evaluated to be one. A linear plot of $k'_{HAT,obs}$ (= k_{HAT}[Rh(tmp)H]) against [TEMPO] revealed a first-order reaction in [TEMPO] (Figure 6). The rate law conformed to: rate = k_{HAT} [Rh(tmp)H] [TEMPO] where k_{HAT} = 0.21 L mol^{-1} s^{-1}. The rates were also measured in the temperature range from 15 to 30 °C and the data are tabulated in Table 6. An Eyring plot (Figure 7) gave the corresponding enthalpies and entropies of activation: $\Delta H_{HAT}^{\ddagger}$ = 21.90 ± 0.33 kcal mol^{-1} and $\Delta S_{HAT}^{\ddagger}$ = 14.43 ± 0.26 cal K^{-1} mol^{-1}.

The second-order kinetics suggest a direct hydrogen atom transfer from [Rh^{III}(tmp)H] to TEMPO in the transition state. The positive value of $\Delta S^{\ddagger}_{HAT}$ is rather intriguing, and may indicate a dissociative activation process, perhaps related to breaking of the Rh−H bond. A bimolecular associative mechanism is not consistent with these data. However, the obtained rate constant k_{HAT} might not be an elementary one, and we have no further mechanistic information. Besides a direct HAT

Table 4. Observed Rate Constants k_{obs} at Different Temperatures

entry	T (°C)	$1/T$ (K^{-1})	k'_{obs} (10^{-4} s^{-1})	k_{obs} (L mol^{-1} s^{-1})	$\ln(k_{obs}/T)$
1	50.0	0.00310	0.772 ± 0.005	0.0233	−9.537
2	55.0	0.00305	1.107 ± 0.009	0.0334	−9.192
3	60.0	0.00300	1.698 ± 0.002	0.0512	−8.779
4	70.0	0.00292	3.497 ± 0.075	0.1056	−8.086
5	75.0	0.00287	5.217 ± 0.014	0.1575	−7.701
6	80.0	0.00283	6.969 ± 0.022	0.2104	−7.425

Table 5. $k'_{HAT,obs}$ under Different Rh(tmp)H Concentrations at 15 °C

entry	[Rh(tmp)H] (×10^{-5} M)	[TEMPO] (×10^{-4} M)	$k'_{HAT,obs}$ (×10^{-4} s^{-1})
1	2.958	9.108	1.965 ± 0.042
2	5.916	9.108	1.944 ± 0.041
3	8.874	9.108	1.973 ± 0.032
4	5.916	18.22	4.022 ± 0.073
5	5.916	27.32	6.267 ± 0.018
6	5.916	36.43	8.256 ± 0.026
7	5.916	54.65	13.21 ± 0.028

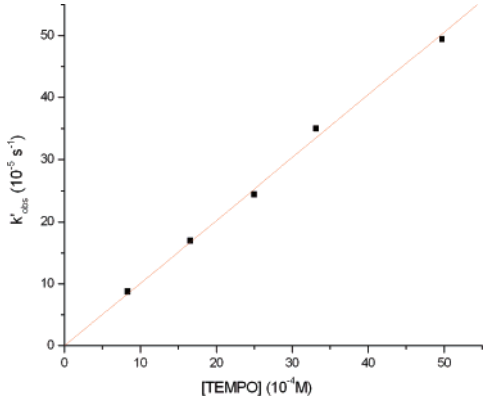

Figure 5. Linear relationship between k'_{obs} and [TEMPO].

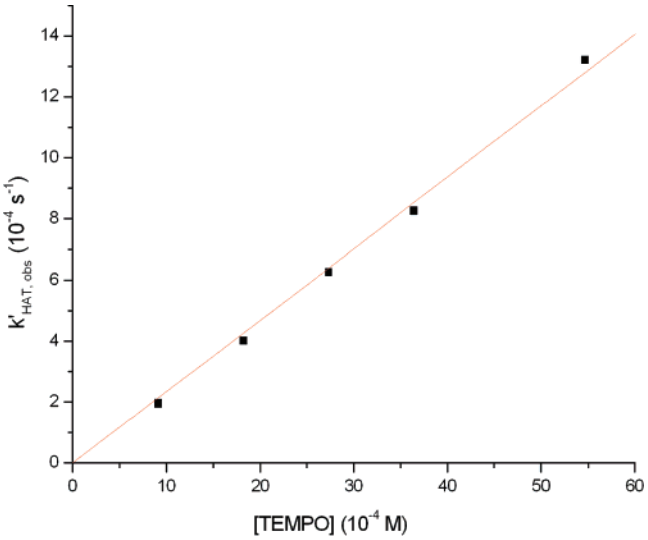

Figure 6. Linear relationship between $k'_{HAT\ obs}$ and [TEMPO].

reaction, a proton coupled electron transfer (PCET)[14] might be operative. We are currently working on obtaining kinetic isotope data and DFT calculations for this reaction, to be published in a separate paper. In this paper we further focus on the mechanistic details of the CCA (and necessarily the competing CHA).

(14) For a leading reference of PCET, see: Rhile, I. H.; Mayer, J. M. *Angew. Chem., Int. Ed.* **2005**, *44*, 1598−1599.

Table 6. Temperature Dependent Observed Rate Constant $k'_{HAT,obs}$ and k_{HAT}

temp (°C)	$1/T$ (K^{-1})	$k'_{HAT,obs}$ (10^{-4} s^{-1})	k_{HAT} (L mol^{-1} s^{-1})	$\ln(k_{HAT}/T)$
15.0	0.00347	1.94 ± 0.04	0.2134	−7.2074
20.0	0.00341	3.68 ± 0.07	0.4045	−6.5853
25.0	0.00336	6.70 ± 0.12	0.7358	−6.0038
30.0	0.00330	13.2 ± 0.18	1.4493	−5.3427

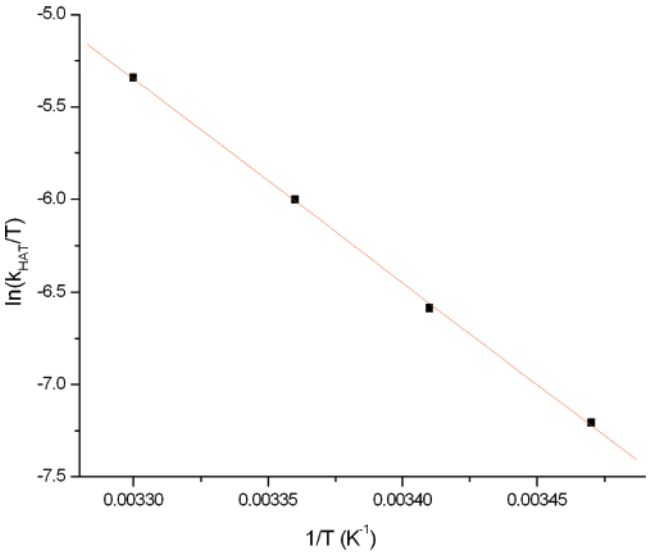

Figure 7. Eyring plot of reaction between Rh(tmp)H and TEMPO.

It is clear that the measured hydrogen atom transfer rate constant k_{HAT} (0.21 L mol^{-1} s^{-1} at 15 °C) is much larger than the overall rate constant for the competing CCA and CHA reactions k_{obs} (0.11 L mol^{-1} s^{-1} at 70 °C). So clearly the preceding CHA and CCA steps are rate-limiting in the two competing pathways.

The extrapolated binding constant K_1 for TEMPO binding to [Rh^{II}(tmp)] (488 M^{-1}) is still relatively large even at 70 °C. This binding constant implies that up to 70% of [Rh^{II}(tmp)] is associated with TEMPO as the adduct [Rh(tmp)(TEMPO)] **8** under the applied reaction conditions. The rate equation: rate $= \{(k_2 + k_3)K_1[\text{TEMPO}][\text{Rh(tmp)}]_0\}/\{1 + K_1[\text{TEMPO}]\}$ would apply for competitive CHA and CCA reactions each proceeding via **8** (without subsequent isomerization of **8** to **8′**, see Supporting Information for a derivation). This equation cannot be further simplified (with $K_1[\text{T}] = 488\ M^{-1} \times 3.313 \times 10^{-3}\ M = 1.61$ being of the same order as one) and such the binding constant $K_1 = 488\ M^{-1}$ would without doubt lead to saturation kinetics if the rate-limiting steps would follow directly from **8**. This is not compatible with the clear experimental first-order kinetic behavior in both [TEMPO] and [[Rh^{II}(tmp)]]$_0$. This implies that formation of **8** might not be productive, or its formation is followed by subsequent reaction with a much smaller equilibrium constant K_2. We considered the possibility that the Rh(tmp)-η^1-*O*-TEMPO complex **8** could react with another molecule of TEMPO to undergo the CCA and CHA reactions. However, kinetic modeling would yield the rate equation: rate $= \{(k_2 + k_3)K_1[\text{TEMPO}][\text{Rh(tmp)}]_0\}\ [\text{TEMPO}]/\{1 + K_1[\text{TEMPO}]\}$ (Supporting Information (SI), eq 16 and

Scheme 2 Kinetic Pathways for CCA and CHA of TEMPO by [Rh^{II}(tmp)] Consistent with the Experimental Data

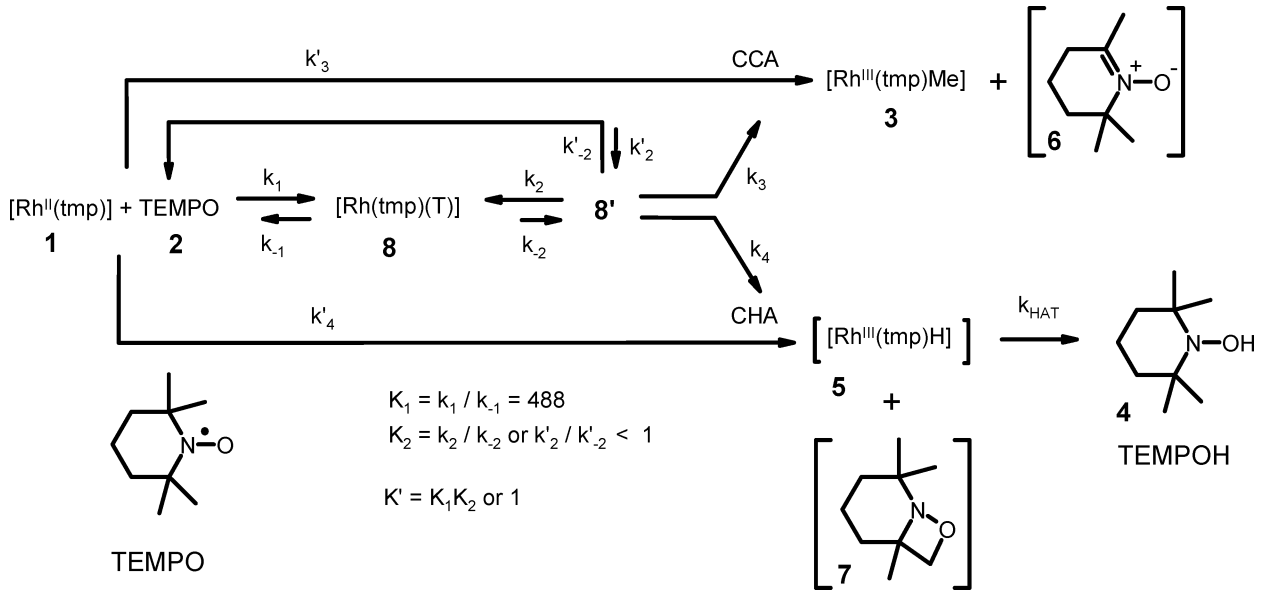

17), which also cannot be further simplified and, more importantly, is not consistent with the observed first-order kinetics in [TEMPO].

This leaves two possibilities each for both the CCA and CHA pathways: (I) formation of **8** is not productive, and the reaction proceeds without any pre-coordination of TEMPO to Rh, or (II) formation of **8** is followed by a subsequent equilibration step **8** ↔ **8′** with a much smaller equilibrium constant K_2 (Scheme 2).[15] If we leave all remaining possibilities open we arrive at the generalized rate equation: rate = $(k_3K_1K_2 + k'_3 + k_4K_1K_2 + k'_4)$[TEMPO][Rh(tmp)]$_0$, which conforms to the experimentally derived rate eq 3 with $k_{obs} = (k_3K_1K_2 + k'_3 + k_4K_1K_2 + k_4)$. Although the k_3 and k'_3 pathways are not likely to have similar rate constants, and k_4 and k'_4 are neither likely to be of the same order, the data do not allow us to discriminate between the possible pathways ($k'_n \gg k_nK_1K_2$ vs $k_nK_1K_2 \gg k'_n$). In any case, given the product distributions (Table 1), the kinetics must be dominated by the CCA pathway ($k_{obs} \approx k_3K_1K_2 + k'_3$).

Although the carbon−carbon activation of TEMPO by [Rh(tmp)] may well proceed without pre-coordination, it is noteworthy that all substrates for which CCA by [Rh(tmp)] has been observed are coordinating ones, such as ketones,[10c] amides,[10d] esters,[10d] and nitriles.[10e,f] Metalloradical aliphatic carbon−carbon activation of non-coordinating organic compound has not been reported yet. Several reports of CHA by [Rh^{II}(por)] species have been reported (for an overview, see ref 8a), and we cannot rule out the direct hydrogen abstraction $k_{4'}$ pathway for CHA of TEMPO, as even the C−H bonds of the "non-coordinating" CH_4 can be cleaved between two [Rh^{II}(tmp)] radicals.[6]

The above **8** ↔ **8′** and **1** + **2** ↔ **8′** equilibria, possibly relevant for the unusual CCA pathway, could involve TEMPO η^2-*O*,*N*-side-on binding instead of the expected η^1-*O* end-on binding mode, for which a couple of precedents have been reported.[16] The hindered tetramesityl porphyrin is however expected to impose a rather unfavorable steric constrain for this binding mode. The influence of steric hindrance is illustrated by reported change in the TEMPO coordination modes: while TEMPO is η^2-N,O coordinated in $TiCl_3$(TEMPO),[16i] its is η^1-*O* coordinated in the more hindered complex $CpTiCl_2$(TEMPO).[16e] η^2-*N*.*O* TEMPO coordination to Rh(tmp) might thus not be favorable. Heterolytic Rh−O bond splitting and electron transfer are possible alternatives for these equilibria.

DFT Calculations. The reaction mechanism of the experimentally observed methyl transfer from TEMPO to [Rh^{II}(por)] was further investigated with DFT. We used nonfunctionalized rhodium−porhyrinato complexes [Rh(por)] as model compounds for the experimental [Rh(tmp)] systems.

We first considered a two-step mechanism, in which TEMPO first splits into a methyl radical and the DMPO-like product 2,2,6-trimethyl-2,3,4,5-tetrahydro-1-pyridiniumolate via homolytic C−C bond cleavage, which could then be followed by capture of the methyl radical by [Rh^{II}(por)]. The first step of this mechanism is prohibitedly endergonic according to the DFT calculations (Scheme 3).

However, the calculations do reveal that the respective TEMPO C−C_{Me} bond is rather weak, with an overall thermodynamic bond dissociation enthalpy (BDE) of only +32 kcal/mol (compared to BDE values >60 kcal/mol for regular alkane

(15) In case of rate limiting steps following formation of species **8′**, K_2 must be relatively small (<1) so to make K_1K_2[TEMPO] ≪ 1, thus simplifying the individual rate equations rate = $\{k_nK_1K_2$[TEMPO][Rh(tmp)]$_0\}/\{1 + K_1K_2$-[TEMPO]$\}$ to rate = k_{obs}[T][Rh(tmp)]$_0$ (with $k_{obs} = k_nK_1K_2$ and $n = 3$ or 4).

(16) For references of TEMPO-transition metal complexes: (a) η^1-*O*-(neutral) Rh(II) complex: Felthouse, T. R.; Dong, T.-Y.; Hendrickson, D. N.; Shieh, H.-S.; Thompson, M. R. *J. Am. Chem. Soc.* **1986**, *108*, 8201−8214. (b) η^1-*O*(neutral)−Cu(II) complex: Baskett, M.; Lathi, P. M.; Palacio, F. *Polyhedron*, **2003**, *22*, 2363−2374. (c) η^1-*O*(neutral)−Ru(II) porphyrin: Selyer, J. W.; Fanwick, P. E.; Leidner, C. R. *Inorg. Chem.* **1992**, *31*, 3699−3700. (d) η^1-*O*(anionic)−Si(IV) porphryin: Zheng, J.-Y.; Konishi, K.; Aida, T. *J. Am. Chem. Soc*. **1998**, *120*, 9838−9843. (e) η^1-*O*(anionic)−Ti(IV) complex: Mahanthappa, M. K.; Huang, K.-W.; Cole, A. P.; Waymouth, R. M. *Chem. Commun.* **2002**, 502−503. (f) η^1-*O*(anionic)−Ir(III) complex: Hetterscheid, D. G. H.; Kaiser, J.; Reijerse, E.; Peters, T. P. J.; Thewissen, S.; Blok, A. N. J.; Smits, J. M. M.; de Gelder, R.; de Bruin, B. *J. Am. Chem. Soc*. **2005**, *127*, 1895−1905. (g) η^1-*O*(anionic)-μ-η^1:η^2−*ON* Sm(III) complex: Evans, W. J.; Perotti, J. M.; Doedens, R. J.; Ziller, J. W. *Chem. Commun*. **2001**, 2326−2327. (h) η^2-*O(anionic)N*−Ni(II) complex: Mindiola, D. J.; Waterman, R.; Jenkins, D. M.; Hillhouse, G. L. *Inorg. Chim. Acta* **2003**, *345*, 299−308. (i) η^2-*O (anionic)N*−Ti(IV) complex: ref 16e.

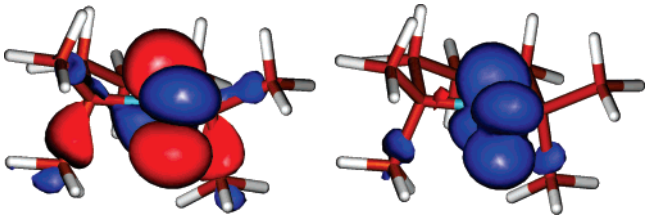

Figure 8. SOMO (left) and spin density (right) plots of TEMPO, revealing significant unpaired electron density at the "axial" methyl fragments (b3-lyp, TZVP).

Scheme 3. Calculated Standard Free Energies (kcal/mol), Standard Enthalpies (kcal/mol), Standard Entropies (cal·mol^{-1}·deg^{-1}) and Bond Distances Associated with Methyl Radical Dissociation from TEMPO (Homolytic C−C Bond Splitting, b3-lyp, TZVP)

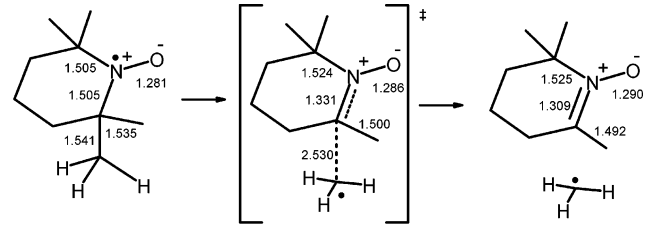

ΔG⁰	=0	+38.9	+18.9
ΔH⁰	=0	+40.1	+32.1
ΔS⁰	=0	+4.1	+44.5

Table 7. Energies and Free Energies Associated with the Calculated Reaction Paths for Me Transfer from TEMPO to [Rh^{II}(por)]

	I[c]	II[d]	TS1[e]	III[d]	TS2[d]	IV[d]
ΔE bp86, SVP[a]	+10.7	= 0	-	+13.9	+20.4	−5.0
ΔE b3-lyp, TZVP[a]	−7.2	= 0	+14.3	+15.7	+22.7	−13.8
ΔG^0_{298K} b3-lyp[b]	−18.2	= 0	+11.7	+11.5	+17.0	−23.6
ΔG_{353K} b3-lyp[b]	−16.6	= 0	+11.7	+11.6	+17.4	−22.6

[a] Energies (kcal/mol). [b] Free energies (kcal/mol) corrected for dielectric solvent effects (COSMO, $\epsilon = 2.28$). [c] Two gas phase separated doublets. [d] Singlet. [e] Open-shell singlet (singlet biradical): broken symmetry, unrestricted b3-lyp solution.

C−C bonds). This is clearly the result of concerted formation of a C=N π-bond associated with the homolytic C−C splitting.

The calculations did reveal a significant spin density located at the two "axial" methyl fragments of TEMPO, caused by some (antibonding) mixing-in of the respective C−C bonding orbitals with the half-filled N−O π^* orbital (see Figure 8). This insight led us to investigate a direct methyl radical transfer pathway from TEMPO to [Rh^{II}(por)] along the "broken symmetry" (unrestricted b3-lyp, open-shell singlet) singlet biradical potential surface (i.e., a bimolecular homolytic substitution; S_H2). The experimental results clearly reveal that TEMPO binds to [Rh^{II}(por)], with the kinetics not being conclusive whether this is a productive step in the formation of the final [Rh^{III}(por)Me] product, or not. Therefore we also considered an alternative pathway, proceeding via the [TEMPO]$^+$ [Rh^{I}(por)]$^-$ cation−anion pair, obtainable via electron transfer from the TEMPO radical to [Rh^{II}(por)] (**I**) or via heterolytic bond splitting of the Rh−O bond of the TEMPO adduct (**II**), respectively (Scheme 4).[17] The energies associated with the species depicted in Scheme 4 are shown in Table 7.

The binding of TEMPO to rhodium could in principle involve formation of the expected η^1-*O*-bound TEMPO adduct **II** (Scheme 4), or alternatively its η^1-*N*-bound or η^2-*N,O*-bound isomer. Attempts to optimize (singlet) η^1-*N*-bound or η^2-*N,O*-bound TEMPO adducts all converged to the η^1-*O*-bound TEMPO adduct **II**. The optimized geometry of **II** corresponds well with our previously reported diamagnetic η^1-*O*-bound TEMPO-Ir^{III} adduct formed from TEMPO and an Ir^{II} species.[16f] Optimizing complex **II** in a triplet spin state led to TEMPO dissociation from Rh, and (broken symmetry) attempts to optimize **II** as singlet biradical did not lead to a lower energy. The energy values associated with TEMPO capture by the [Rh^{II}(por)] radical to form the diamagnetic η^1-*O*-bound TEMPO adduct [Rh^{III}(por)(TEMPO)] **II** are not reliable, since they involve comparing systems of different spin states.[18−20] This problem is evident from the calculated *exothermicity* of formation of **II** at the bp86-SV(P) level (in reasonable agreement with the experimentally derived $\Delta G^0 = -5.3$ kcal/mol value associated with TEMPO binding), while at the b3-lyp-TZVP level of theory formation of **II** from the TEMPO and [Rh^{II}(por)] radicals is endothermic. Apparently, the hybrid b3-lyp functional overestimates the relative stability of the separated radicals.[20] Relative energies of the (closed-shell) singlet species formed *after* the TEMPO capture to form **II** should be more reliable, and for these subsequent steps we found no large differences between the bp86 and b3-lyp levels of theory. We thus decided to take the TEMPO adduct **II** as a reference point for comparing the relative energies (corresponding with the experimental data).

(17) Electron transfer from TEMPO to [Rh^{II}(por)] (formation of **III**, Scheme 4) is noteworthy. [Rh^{II}(por)] species and nitroxyl radicals are both redox active and both have the ability to act as reducing *and* as oxidizing agents. The reverse SET direction (from Rh to TEMPO) seems applicable in the formation of the TEMPO adduct [Rh^{III}(por)(TEMPO$^-$)] **II**. Hypothetical *outer-sphere* ET from [Rh^{II}(tmp)] to TEMPO would yield a [Rh^{III}(por)]$^+$[TEMPO]$^-$ cation−anion pair. This is perhaps possible in polar solvents, but in the gas-phase or in benzene it would easily collapse to form the [Rh(por)(TEMPO)] adduct **II**. In previous reports, we have already shown that the methyl transfer reaction cannot proceed via reaction of neutral nitroxyl radicals with [Rh^{III}(por)]$^+$ cations or [Rh^{I}(por)]$^-$ anions.[10b]

(18) Gosh, A. *J. Biol. Inorg. Chem.* **2006**, *11*, 712−724.

(19) Harvey, J. N.; Poli, R.; Smith, K. M. *Coord. Chem. Rev.* **2003**, *238−239*, 347−361.

(20) This is not the first time that hybrid HF/DFT functionals (such as b3-lyp) are found to overestimate the relative stability of radicals compared to closed-shell systems: (a) Saeys, M.; Reyniers, M.-F.; Marin, G. B.; Van Speybroeck, V.; Waroquir, J. *Phys. Chem. A* **2003**, *107*, 9147−9159. (b) Sustmann, R.; Sicking, W.; Huisgen, R.; *J. Am. Chem. Soc.* **2003**, *125*, 14425−14434. (c) Jensen, K. P.; Ryde, U.; *J. Phys. Chem. A* **2003**, *107*, 7539−7545. (d) Gosh, A.; *J. Biol. Inorg. Chem.* **2006**, *11*, 712−724.

(21) (a) Ozinskas, A. J.; Bobst, A. M. *Helv. Chim. Acta* **1980**, *63*, 1407−1411. (b) Fields, J. D.; Kropp, P. J. *J. Org. Chem.* **2000**, *65*, 5937−5941.

(22) Wayland, B. B.; Van Voorhees, S. L.; Wilker, C. *Inorg. Chem.* **1986**, *25*, 4039−4042.

(23) Perkampus H. H. *UV-VIS Spectroscopy and Its Applications*; Springer-Verlag: Berlin, Heidelberg, 1992.

(24) Atkins, P. *Physical Chemistry*, 6th ed.; Oxford University Press: Oxford, U.K., 1998.

(25) (a) Ahlrichs, R; et al. *Turbomole*, version 5; Theoretical Chemistry Group, University of Karlsruhe: Karlsruhe, Germany, 2002. (b) Treutler, O.; Ahlrichs, R. *J. Chem. Phys.* **1995**, *102*, 346−354. (c) *Turbomole*, version 5, Turbomole basisset library (see ref 25a). (d) Schäfer, A.; Horn, H.; Ahlrichs, R. *J. Chem. Phys.* **1992**, *97*, 2571−2577. (e) Andrae, D.; Haeussermann, U.; Dolg, M.; Stoll, H.; Preuss, H. *Theor. Chim. Acta* **1990**, *77*, 123−141. (f) Schäfer, A.; Huber, C.; Ahlrichs, R. *J. Chem. Phys.* **1994**, *100*, 5829−5835. (g) Ahlrichs, R.; May, K. *Chem. Phys.* **2000**, *2*, 943.

(26) (a) *PQS*, version 2.4; Parallel Quantum Solutions: Fayetteville, AR, 2001 (the Baker optimizer is available separately from PQS upon request). (b) Baker, J. *J. Comput. Chem.* **1986**, *7*, 385−395.

(27) (a) Becke, A. D. *Phys. Rev. A* **1988**, *38*, 3098−3100. (b) Perdew, J. P. *Phys. Rev. B* **1986**, *33*, 8822−8824.

(28) (a) Lee, C.; Yang, W.; Parr, R. G. *Phys. Rev. B* **1988**, *37*, 785−789. (b) Becke, A. D. *J. Chem. Phys.* **1993**, *98*, 1372−1377. (c) Becke, A. D. *J. Chem. Phys.* **1993**, *98*, 5648−5652. (d) Calculations were performed using the Turbomole functional "b3-lyp", which is not identical to the Gaussian "B3LYP" functional.

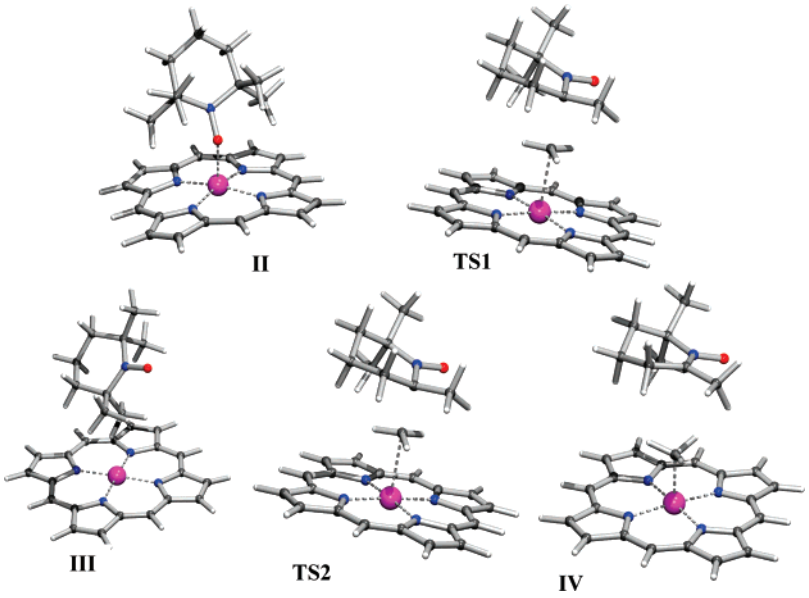

Figure 9. DFT optimized geometries (b3-lyp, TZVP) of **II**, **TS1**, **III**, **TS2**, and **IV**.

Scheme 4. Computational Reaction Mechanisms for Methyl Transfer from TEMPO to [Rh^{II}(por)], in Good Agreement with the Experimental Kinetic Data

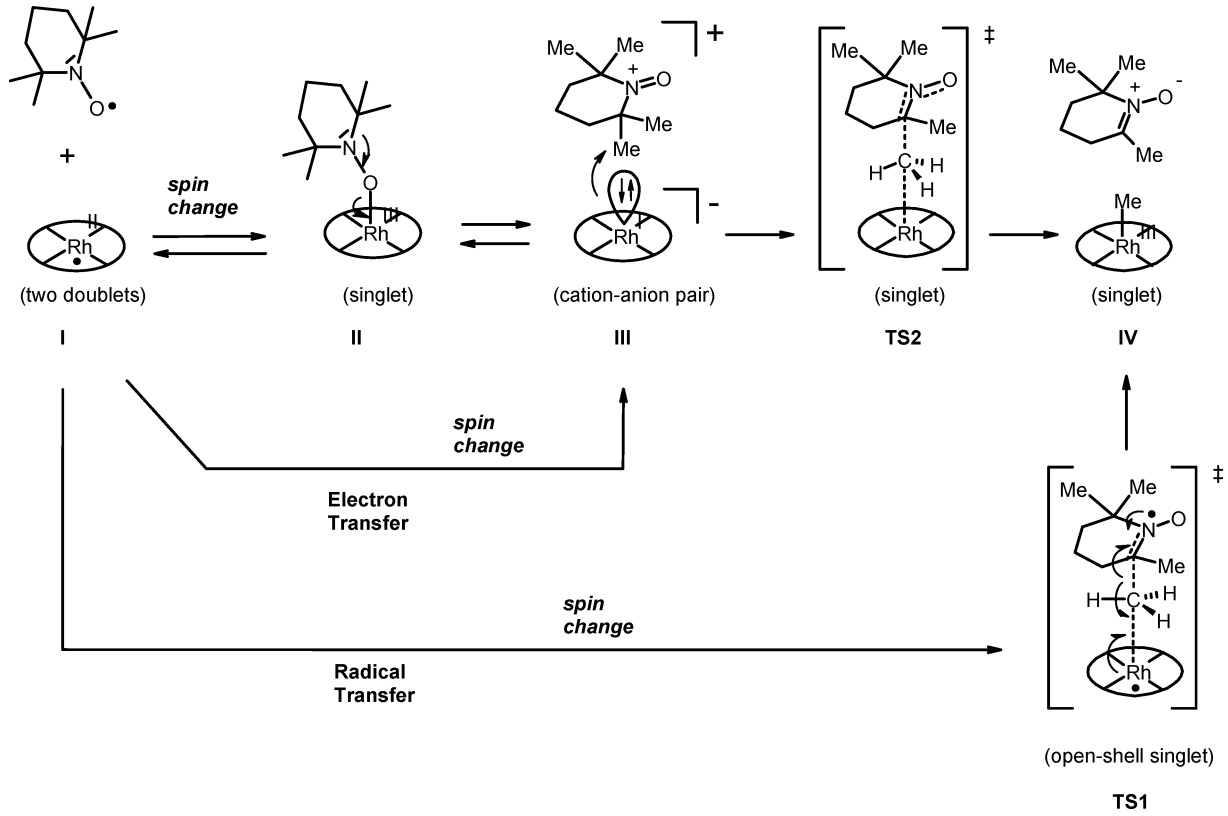

Formation of the cation−anion pair **III** from **II** is about +12 kcal/mol uphill. From this cation−anion pair we readily obtained an S_N2-like transition state (**TS2**) for methyl transfer from TEMPO to Rh. This transition state involves a nucleophilic attack of the electron rich Rh^I atom to one of the methyl groups of the TEMPO cation, with (DMPO-like) 2,2,6-trimethyl-2,3,4,5-tetrahydro-1-pyridiniumolate acting as an efficient leaving group (S_N2 type mechanism, see Scheme 4). **TS2** lays only about +17 kcal/mol uphill with respect to **II**. Formation of the final products **IV** from **II** is exergonic by nearly −24 kcal/mol.

The transition state for direct Me radical transfer from the TEMPO radical to the [Rh^{II}(por)] radical (S_H2-type mechanism), along the open-shell singlet (singlet biradical) surface, has an even lower relative energy ($\Delta G^{\ddagger} = +12$ kcal/mol). On this basis, the actual reaction might well take place via direct methyl radical transfer (**TS1**) instead of the alternative ionic pathway (**TS2**). However, the hybrid b3-lyp functional seems to overestimate the relative stability of radicals.[20] It is not so clear if, and to what extend, this also holds for the singlet biradicaloid transition state **TS1** (which is "on the way" to become closed-shell; $\langle S^2 \rangle$

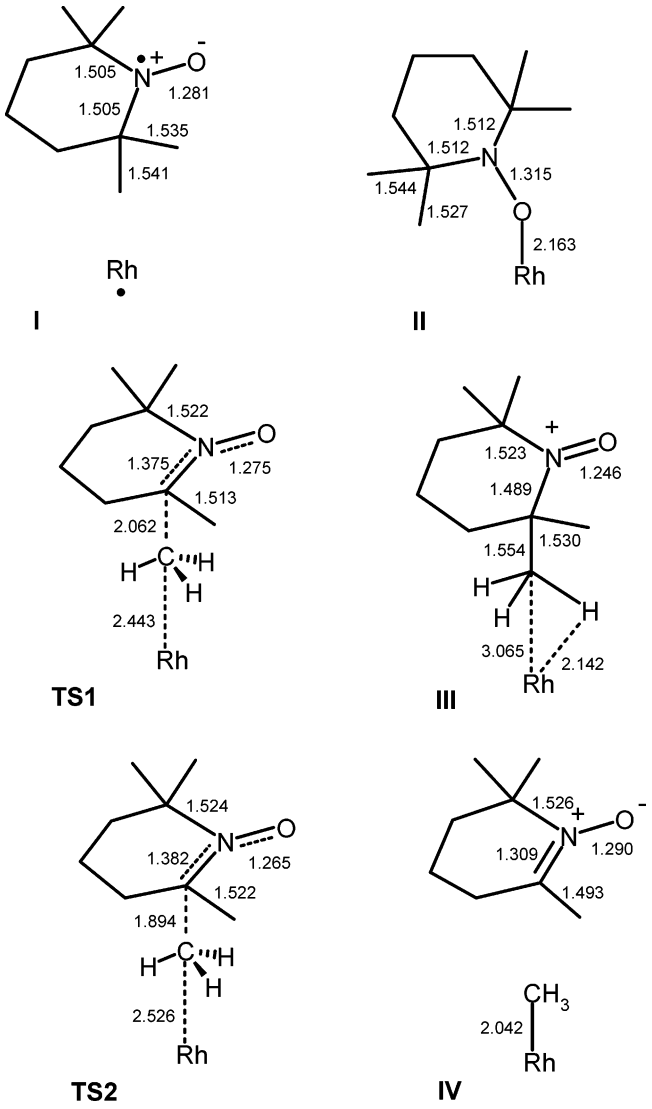

Figure 10. Selected bond-length changes associated with the methyl group transfer pathways.

= 0.47). It might well be that the stability of **TS1** relative to **TS2** is also overestimated. This seems to be supported by the fact that at the (pure DFT) bp86 level of theory, **TS1** does not exist (all attemps to find **TS1** at the (u)bp86 level led to **TS2**). On the other hand, the computational restrictions associated with single determinant (u)b3-lyp optimization of **TS1** unavoidably led us to optimize its geometry as a mixture of its real (multideterminant singlet biradical) electronic structure and its triplet state.[29] This is likely to result in a too high energy. To what extent these effects counterbalance is not clear, and therefore we are unable to reliably distinguish between the ionic (**TS2**) and direct radical abstraction (**TS1**) pathways on the basis of these DFT calculations.

The optimized geometries of **II**, **III**, **IV**, **TS1**, and **TS2** are depicted in Figure 9. The bond length changes are represented in Figure 10, which require some additional comments. It is clear that the N−O bond distance reflects the "oxidation state" of the TEMPO moiety. Going from **I** to **II**, the TEMPO moiety is reduced by one electron, which decreases the N−O bond order from 1.5 to 1. The "oxidized" TEMPO moiety in **III** has no electrons in the N−O π^* antibonding orbital, leading to a net bond order of 2. The nucleophilic attack of Rh^I at the oxidized TEMPO of **III** leads to a net "reduction" with formation of the (DMPO-like) nitrone 2,2,6-trimethyl-2,3,4,5-tetrahydro-1-pyridiniumolate of **IV** via **TS2**. As expected, the N−O bond distances increase and the C−N bond distances decrease along the (S_N2-type) ionic pathway from **III** via **TS2** to **IV**. However, the changes of bond distances along the (S_H2-type) radical pathway **I** → **TS1** → **IV** are less clear. On going from **I** to **TS1** the N−O bond distance first decreases to eventually become even longer in **IV** (compared to **I**). It is clear that **TS1** is optimized as a mixture of the "real" singlet biradical and its triplet state. This is one possible explanation for the observed discrepancy in the behavior of the N−O bond lengths. Another possible explanation is that some partial electron transfer from TEMPO to Rh also occurs in **TS1**, giving rise to a shortening of the N−O distance in the transition state.

The obtained barriers **TS1** and **TS2** for the ionic (S_N2) and the direct radical transfer (S_H2) pathways are rather low, suggesting that the reaction might even proceed at room temperature. However, considering the fact that the experimental [Rh^{II}(tmp)] system is sterically much more shielded, the calculated mechanistic pathways seem both qualitatively and quantitatively in good agreement with the experimental results. Since both pathways are consistent with the experimental kinetic data, we are not able to make a distinction (neither experimentally nor computationally) between these two possibilities.

Conclusions

Major carbon−carbon bond activation (CCA) and minor carbon-hydrogen bond activation (CHA) in reaction between rhodium(II) meso-tetramesitylporphyrin Rh(tmp) **1** and 2,2,6,6-tetramethyl-piperidine-1-oxyl (TEMPO) **2** are both associated with first-order kinetics in TEMPO and [Rh^{II}(tmp)]. The selectivity for CCA increases at higher temperatures. U-DFT reveals a low-energy transition state (**TS1**) for direct abstraction of a methyl radical from TEMPO by the Rh^{II} radical (S_H2-type mechanism). R-DFT reveals an alternative ionic pathway along the closed-shell singlet surface. This ionic pathway proceeds in two sequential steps: electron transfer from TEMPO to [Rh^{II}(por)] producing the $[TEMPO]^+[Rh^I(por)]^-$ cation−anion pair, followed by CH_3^+ transfer from $TEMPO^+$ to Rh^I with formation of [Rh^{III}(por)Me] and a (DMPO-like) 2,2,6-trimethyl-2,3,4,5-tetrahydro-1-pyridiniumolate leaving group. The transition state for this process (**TS2**) is best described as an S_N2-like nucleophilic substitution involving attack of the d_z2 orbital of $[Rh^I(por)]^-$ at a C−C σ^* orbital of $[TEMPO]^+$. The R-DFT and U-DFT calculations are comparatively not accurate enough to reliably distinguish between these possible pathways. Both the radical (S_H2) and the ionic (S_N2) pathway have barriers which are low enough to explain the experimental data, and both pathways are consistent with the experimental kinetic data. These remarkable and unprecedented reactivity patterns for TEMPO suggest that TEMPO can act as methyl radical donor, a reducing agent, and (in its oxidized form) as a CH_3^+ donor to (late) transition metals. Since TEMPO is often used as a radical inhibitor in various (catalytic) reactions, the possible implications of these new insights need to be further explored.

(29) Knijnenburg, Q.; Hetterscheid, D.; Kooistra, T. M.; Budzelaar, P. H. M.; *Eur. J. Inorg. Chem.* **2004**, 1204−1211 and references cited therein.

Experimental Section

All chemicals were purchased from commercial suppliers and used without further purification unless otherwise specified. Dichloromethane was distilled from calcium hydride under nitrogen. Chloroform was distilled from calcium chloride under N_2. Hexane was distilled from calcium chloride. Benzene was distilled from sodium under N_2. 1,2-Dichloroethane was distilled from calcium hydride under N_2. 2,2,6,6-Tetramethyl-pyperidin-1-oxyl (TEMPO) was purified by vacuum sublimation.

Thin layer chromatography was performed on Merck precoated silica gel 60 F_{254} plates. Column chromatography was performed on silica gel (70−230) or neutral aluminum oxide (activity I, 70−230 mesh).

^{1}H NMR spectra were recorded on a Bruker DPX-300 (300 MHz). Chemical shifts were referenced with the residual solvent protons in C_6D_6 (δ 7.15 ppm), $CDCl_3$ (δ 7.24 ppm), or with tetramethylsilane (δ 0.00 ppm) as the internal standard. Chemical shifts (δ) were reported as part per million (ppm) in δ scale.

Gas chromatography was performed on a HP G1800 GCD system using a HP5MS column (30 m × 0.25 mm × 0.25 μm).

UV−vis spectra were performed on a Hitachi U-3300 spectrophotometer equipped with a Neslab temperature circulator RTE-110 for temperature control with a mixture of ethylene glycol and water (v/v = 1/1) used as the circulating liquid. The temperature was measured by a Fluke thermometer connected to a K-type thermal couple wire placed in an adjacent dummy UV cell filled with benzene. Spectral and rate data were analyzed with OriginPro 7.5 software.

Reaction of [Rh^{II}(tmp)] with TEMPO. To a Teflon screw-head stoppered flask, [Rh^{III}(tmp)CH_3] **3** (10.0 mg, 0.011 mmol) was dissolved in C_6H_6 (4.0 mL) to form a clear orange solution. The reaction mixture was then degassed by the freeze−pump−thaw method (3 cycles) and refilled with N_2. The reaction mixture was irradiated under a 400 W Hg-lamp at 6−10 °C until complete [Rh^{III}(tmp)CH_3] consumption was confirmed by TLC analysis (10−11 h). Benzene solution of [Rh^{II}(tmp)] **1** (0.0088 mmol, 4.0 mL, 80%) was prepared.[6e,10b] Then TEMPO **2** (0.055 mmol) was added to the benzene solution of [Rh^{II}(tmp)] and the reaction mixture was heated under N_2 in the absence of light. After cooling down to room temperature, 1 μL of degassed anthracene solution (0.0749 M) was added as internal standard. The yield of TEMPOH **4** was measured by GC−MS.

The reaction mixture was purified by chromatography on silica gel eluting with a solvent mixture of hexane/CH_2Cl_2 (10:1) to hexane/CH_2Cl_2 (7:1) to give the orange solid of [Rh^{III}(tmp)CH_3] with ^{1}H NMR spectrum identical to that of an authentic sample.

Preparation of TEMPOH 4.[21] To TEMPO **2** (500 mg, 3.2 mmol), a 1:1 mixture of acetone/water (60 mL) and 85% $Na_2S_2O_4$ (717 mg, 3.5 mmol) were added. The orange solution decolorized instantly upon swirling. After stirring for 0.5 h at room temperature, acetone was removed under reduced pressure. The remaining aqueous solution was extracted with degassed diethylether under N_2. Then the ether extract was dried over K_2CO_3 under N_2. The solution was filtered under N_2 using a cannular with the tip wrapped with a filter paper. Then the solvent was removed under high vacuum. White solid (392 mg, 2.5 mmol, 78%) was obtained. ^{1}H NMR (C_6D_6, 300 MHz): δ 1.16 (s, 6 H), 1.31 (m, 2 H), 1.38 (m, 4 H), 3.86 (s, 1 H). GCD (column program: initial temperature 70 °C, duration 1 min; increment rate 40 °C/min, duration 3 min; increment rate 45 °C/min, duration 2 min; increment rate 10 °C/min, duration 1 min; final temperature 290 °C, duration 3 min) t_R = 3.87 min; EIMS: m/z 157.

Preparation of (5,10,15,20-Tetramesitylporphyrinato)hydrido Rhodium(III) [Rh^{III}(tmp)H] (5).[10f,22] A red suspension of Rh(tmp)I (50 mg, 0.049 mmol) in EtOH (40 mL) and a solution of $NaBH_4$ (7.5 mg, 0.20 mmol) in aq NaOH (0.5 M, 2 mL) were purged with N_2 separately for about 15 min. The solution of $NaBH_4$ was added slowly to the suspension of [Rh^{III}(tmp)I] via a cannular. The reaction mixture was heated at 55 °C for 3 h and the color changed to deep brown in color. The reaction mixture was then cooled down to 0 °C under N_2, and HCl (40 mL, 0.1 M) was added via syringe. An orange suspension formed immediately and was stirred for 15 min at 0 °C. The workup was carried out under N_2. The reaction mixture was worked up by the addition with degassed benzene/H_2O. The crude product was extracted with degassed benzene (50 mL), washed with H_2O (10 mL × 3), dried over $MgSO_4$, filtered under N_2 using a cannular with the tip wrapped with a filter paper. Then the solvent was removed under high vacuum. A red solid (41.6 mg, 0.047 mmol, 96%) was obtained. ^{1}H NMR (C_6D_6, 300 MHz): δ −40.07 (d, 1 H, $^1J_{RhH}$ = 45 Hz), 1.80 (s, 12 H), 2.14 (s, 12 H), 2.44 (s, 12 H), 7.10 (s, 4 H), 7.19 (s, 4 H), 8.77 (s, 8 H).

Reaction of TEMPO with [Rh^{III}(tmp)H]. TEMPO (38 mg, 0.24 mmol) was added to Rh(tmp)H (42 mg, 0.048 mmol) in anhydrous C_6H_6 (30 mL) under N_2. The mixture was stirred at room temperature (rt) for 30 min. Then, the reaction mixture was analyzed by GC−MS with anthracene (30 μL, 0.0749 M) as the internal standard, and TEMPOH was obtained in 96% yield. The addition of excess iodine to the reaction mixture yielded Rh(tmp)I (45 mg, 0.045 mmol, 93%) after column chromatography. Assuming the yield to be 100% in the reaction between Rh(tmp) and I_2, the yield of Rh(tmp) was estimated to be 93%.

Kinetic Studies of the Reaction between TEMPO (2) and [Rh^{II}(tmp)] (1). Benzene was freshly distilled over sodium, degassed by the freeze−pump−thaw method (three cycles) and refilled with N_2. To a Teflon screw-head stoppered flask, [Rh^{III}(tmp)CH_3] **3** (10.0 mg, 0.011 mmol) was added carefully. Then dried and distilled C_6H_6 (4.000 mL) was added with a gastight syringe. The reaction mixture was then degassed by the freeze−pump−thaw method (three cycles) and refilled with N_2. The reaction mixture was irradiated under a 400 W Hg-lamp at 6−10 °C until complete consumption of Rh(tmp)CH_3 was confirmed by TLC analysis (10−11 h). Stock benzene solution of [Rh^{II}(tmp)] **1** (2.225×10^{-3} M, 4.000 mL) was prepared. Sublimed 2,2,6,6-tetramethyl-pyperidin-1-oxyl (TEMPO) **2** (0.2595 g) was added to a 5.00 mL volumetric flask and was made to the volume with dried benzene. The solution was transferred to a Teflon screw-head stoppered flask. It was degassed by the freeze−pump−thaw method for three cycles. Then it was refilled with N_2. Stock benzene solution of TEMPO (0.3321 M) was prepared.

UV-visible time scans for monitoring the reaction of [Rh^{II}(tmp)] with TEMPO were carried out with varied initial concentrations of Rh(tmp). The stock benzene solution of Rh(tmp) (2.225×10^{-3} M) and dried benzene were transferred separately to a Teflon-stopped Schlenk UV cell with gastight syringe under N_2. The mixture was stirred 10 min at 70.0 ± 0.2 °C inside the sample compartment. Then the stock benzene TEMPO (0.3321 M) was transferred to the UV cell with a gastight syringe under N_2. The reaction was monitored at 523 nm for 4−5 half-lives.

UV Titration of Coordination between [Rh^{II}(tmp)] (1) and TEMPO (2). Stock benzene solution of TEMPO (25 μL, 0.3321 M) was transferred to a Teflon screw-head stoppered flask with a gastight syringe. Then dried benzene (2.500 mL) was added with a gastight syringe. It was degassed by the freeze−pump−thaw method for three cycles. Then it was refilled with N_2. Stock benzene solution of TEMPO (3.288×10^{-3} M) was prepared. The UV−visible wavelength scan was carried out at 10.0 ± 0.2 °C. The stock benzene solution of [Rh^{II}(tmp)] (100 μL, 2.225×10^{-3} M) was transferred to a Teflon-stopped Schlenck UV cell with a gastight syringe under N_2. Then dried benzene (3.900 mL) was added with a gastight syringe under N_2. The stock benzene solution of TEMPO (3.288×10^{-3} M) was then titrated into the [Rh^{II}(tmp)] solution via a gastight microsyringe in 2.0 μL steps up to a total of 20.0 μL and then in 4.0 μL steps up to a total of 60.0 μL TEMPO solution added under N_2. Finally 50 μL of higher concentration TEMPO solution (0.3321 M) was added to the sample solution to obtain the estimated absorbance for the [Rh(tmp)TEMPO)] complex. The UV spectra were scanned at 600 nm/min between 280 and 700 nm. The

absorbance data at 521 nm for the titration at 15.0, 20.0, 25.0, 30.0 ± 0.2 °C, respectively, were measured for evaluation of binding constants.

The binding constants and the number of TEMPO ligand coordinated to each Rh(tmp) complex were calculated by the equation:[23]

$$\log Kn = \log \frac{A_e - A_m}{A_n - A_e} - n \log[L]$$

where n = no. of TEMPO ligand coordinated to each Rh(tmp), Kn = binding constant, [L] = conc. of TEMPO in the UV sample, A_e is the experimental absorbance measured (volume correction made), A_m is the absorbance of the Rh(tmp) without TEMPO, A_n is the theoretical absorbance obtained for the Rh(tmp)−TEMPO complex (obtained from the absorbance measured for the infinite point with volume correction).

The measured A_e values were corrected for volume change due to the addition of ligand solution and the thermal expansion/contraction by $V_t = V_0(1 + \beta t)$ and $\beta = 0.00372$ (for benzene),[24] where V_0 is the volume before correction, t is the changed temperature and V_t is the volume after correction.

Kinetic Study of the Reaction between TEMPO (2) and [Rh^{III}-(tmp)H] (5). The procedure was the same as UV-visible wavelength scan of the reaction between TEMPO **2** and [Rh^{II}(tmp)] **1**. Stock benzene solution of [Rh^{III}(tmp)H] **5** (2.373×10^{-3} M) and TEMPO **2** (0.3321 M) were prepared. First, UV-visible wavelength scan was carried out. The stock benzene solution of [Rh^{III}(tmp)H] (100 μL, 2.373×10^{-3} M) was transferred to a Teflon-stopped UV cell with a gastight syringe under N_2. Then dried benzene (3.900 mL) was added with a gastight syringe under N_2. The mixture was stirred 10 min at 25.0 ± 0.2 °C inside the sample compartment under N_2. Then stock benzene solution of TEMPO (10 μL, 0.3321 M) was transferred to the UV cell with a gastight syringe under N_2. The experimental concentrations were [[Rh^{III}(tmp)H]] = 5.916×10^{-5} M, [TEMPO] = 9.108×10^{-4} M (15 equiv), temperature = 25.0 ± 0.2 °C. The UV spectra were scanned at 600 nm/min between 280 and 700 nm. The spectra were recorded at 0, 2, 5, 10, 30, 60, 90, and 150 min. From the results of wavelength scan, the rates of reactions were monitored at 522 nm, where maximum absorbance changes occurred.

Second, the UV-visible time scan was carried out. The concentration of [Rh^{III}(tmp)H] was varied. The stock benzene solution of [Rh^{III}(tmp)H] (2.373×10^{-3} M) and dried benzene were transferred separately to a Teflon-stopped UV cell with gastight syringe under N_2. The mixture was stirred 10 min at 15.0 ± 0.2 °C inside the sample compartment. Then the stock benzene TEMPO (0.3321 M) was transferred to the UV cell with a gastight syringe under N_2. The reaction was monitored at 522 nm for 4−5 half-lives.

Finally, the reactions were monitored at 522 nm for 4−5 half-lives at temperatures from 15.0 to 30.0 °C. The stock benzene solution of [Rh^{III}(tmp)H] (100 μL, 2.373×10^{-3} M) was transferred to a Teflon-stopped Schlenck UV cell with a gastight syringe under N_2. Then dried benzene (3.900 mL) was added with a gastight syringe under N_2. The mixture was stirred 10 min at a certain temperature inside the sample compartment under N_2. Then stock benzene solution of TEMPO (10 μL, 0.3321 M) was transferred to the UV cell with a gastight syringe under N_2. The experimental concentrations were [[Rh^{III}(tmp)H]] = 5.916×10^{-5} M, [TEMPO] = 9.108×10^{-4} (15 equiv).

DFT Calculations. The geometry optimizations were carried out with the Turbomole program[25a,b] coupled to the PQS Baker optimizer.[26] Geometries were fully optimized as minima or transition states at the bp86[27] level using the SV(P) basis set[25d] on all atoms (small-core pseudopotential[25c,e] on rhodium and iridium) and at the b3-lyp level[28] using the polarized triple-ζ TZVP basis[25c,f] (small-core pseudopotential[25c,e] on Rh). The "real" energy ϵ_s of the (multideterminant) open-shell singlet **TS1** (singlet biradical) was estimated from the energy ϵ_0 of the optimized single-determinant broken symmetry unrestricted b3-lyp (TZVP) solution ($S_0^2 = 0.454$) and the energy ϵ_1 from a separate unrestricted $m_s = 1$ calculation at the same geometry ($S_1^2 = 2.007$), using the formula[29]

$$\epsilon_s \approx \frac{S_1^2\epsilon_0 - S_0^2\epsilon_1}{S_1^2 - S_0^2}$$

Solvent corrections from single-point cosmo calculations ($\epsilon = 2.28$) were applied for all species.[30] The stationary points optimized at the b3-lyp level (RDFT and UDFT) were characterized by vibrational analysis (numerical frequencies); ZPE and thermal corrections (entropy *and* enthalpy, 298 and 353 K, 1 bar) from these analyses are included. The thus obtained (free) energies (kcal/mol) are reported in Table 7. Optimized geometries of **II**, **III**, **IV**, **TS1**, and **TS2**, visualized with the PLATON[31] program (rendered with POVRAY), are shown in Figure 9. The orbital and spin density plots shown in Figure 8 were generated with Molden.[32]

Acknowledgment. We thank the Research Grants Council of Hong Kong (CUHK 400104) and The Netherlands Organization for Scientific Research (NWO-CW) for financial support. We thank Prof. P. H. M. Budzelaar (Manitoba) and Prof. P.-O. Norrby (Gothenburg) for helpful discussions about the DFT calculations.

Supporting Information Available: Experimental details, kinetic data and derivation of rate laws and activation parameters, complete ref 25a, (u)b3-lyp optimized geometries of **I**, **II**, **III**, **IV**, **TS1**, **TS2**, and the species depicted in Scheme 3. This material is available free of charge via the Internet at http://pubs.acs.org.

JA078157F

(30) Klamt, A.; Schüürmann, G.; *J. Chem. Soc., Perkin Trans. 2* **1993**, *5*, 799−805.
(31) Spek, A. L. *PLATON, A Multipurpose Crystallographic Tool*; Utrecht University: Utrecht, The Netherlands, 2003.
(32) Schaftenaar, G.; Noordik, J. H. *J. Comput.-Aided Mol. Des.* **2000**, *14* (2), 123−134.